Astron. & Astrophys. 29, 135 – 149 (1973)

The β Scorpii Occultation by Jupiter

II. The Temperature and Density Profiles of the Jovian Upper Atmosphere

L. Vapillon, M. Combes and J. Lecacheux
Groupe «Planètes», Observatoire de Meudon

Received June 21, 1973

Summary. The aim of this paper is to present results of temperature and density profiles of the upper atmosphere of Jupiter as deduced from observation of the occultation of β Sco[1]), on May 13, 1971. The experiment and photometric results are briefly described: the occultation light curve of β Sco A was recorded for more than 900 s at immersion and for more than 820 s at emersion. The analysis of data is based on an Abelian integral inversion, the planetary atmosphere being assumed to be spherically symmetric. Jovian refractivity profiles and typical temperature and density profiles are shown.
The extent of the probe of the atmospheric layers is discussed: the upper limit is $h = 30$ km owing to the influence of the boundary constant needed to perform the integral inversion and to the consequences of the uncertainty on the stellar flux before the occultation. The lower limit may be $h = -200$ km because of the influence of an error on the zero light level and because it may be hazardous to maintain the assumption of spherical symmetry for deeper atmospheric layers. Some sources of systematic error are reviewed, namely, the change in star velocity relative to the planet, Jovian ellipticity, variation of the acceleration due to gravity and the role of the magnitude of β Sco B.
Some conclusions concerning the Jovian upper atmosphere are given: the temperature at $h = -100$ km is $T = 220 \pm 30$ °K; the thermal lapse rate between -50 and -150 km is close to -1.5 °K · km^{-1}; and a maximum of temperature (300 to 400 °K) is reached at a pressure close to 1 mb. Above $h = -50$ km, an isothermal layer may exist ($T = 150 \pm 50$ °K). No information about the thermosphere can be obtained.

Key words: Jupiter – occultation – planetary atmospheres

Introduction

In this paper, we present results for the temperature and density profiles of the upper atmosphere of Jupiter as deduced from our observations of the occultation of β Scorpii on May 13, 1971.
The initial analysis of the data has revealed that the mean scale height of the Jovian atmosphere is close to 30 km, that the temperature is close to 200 °K and increases with depth, and that the atmospheric layer we have probed extends to the well-mixed atmosphere and possibly reaches a temperature maximum (Combes *et al.*, 1971). The occultation observations have been used to derive the diameter of Jupiter and correction to its ephemeris (Lecacheux *et al.*, 1972). The photometric measurements, data reduction and a complete description of the instrumentation is given by Berezné *et al.* (1974).
We have now performed a complete analysis of our results for the upper Jovian atmosphere. In Section I, we shall present the basic data: photometric measurements and astrometric computations. In Section II, the method of analysis, based on Abelian integral inversion, will be summarized. In Section III, we shall derive the Jovian refractivity profile and typical related temperature and number density profiles. In Section IV, we shall discuss in some detail the extent of the atmospheric layer which was probed and the limitations due to systematic errors. In Section V, we shall present the most important conclusions concerning the Jovian upper atmosphere. The notation will be defined in Appendix I.

[1]) Observations were made at Radcliffe Observatory – Pretoria (South Africa).

I. Experiment and Photometric Results

a) The Experiment

As we shall see later, the inaccuracy in the determination of the zero-level of star light is the dominant limitation in a stellar occultation experiment. Owing to the close proximity of the star and the planetary limb, a significant part of the flux received by the recording device is due to Jupiter. Because of photon noise, guiding

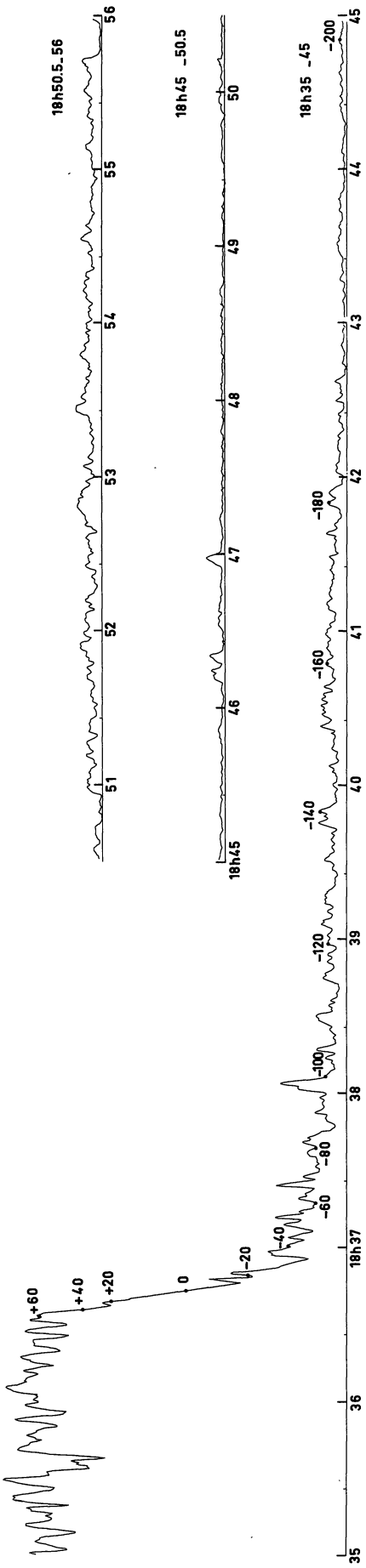

Fig. 1. The light curve, $\Phi(t)$, of β SCO A at Immersion, from 18 h 35 to 18 h 56 (U.T.). The altitudes h corresponding to the points of closest approach are marked at 20 km intervals down to $h = -200$ km

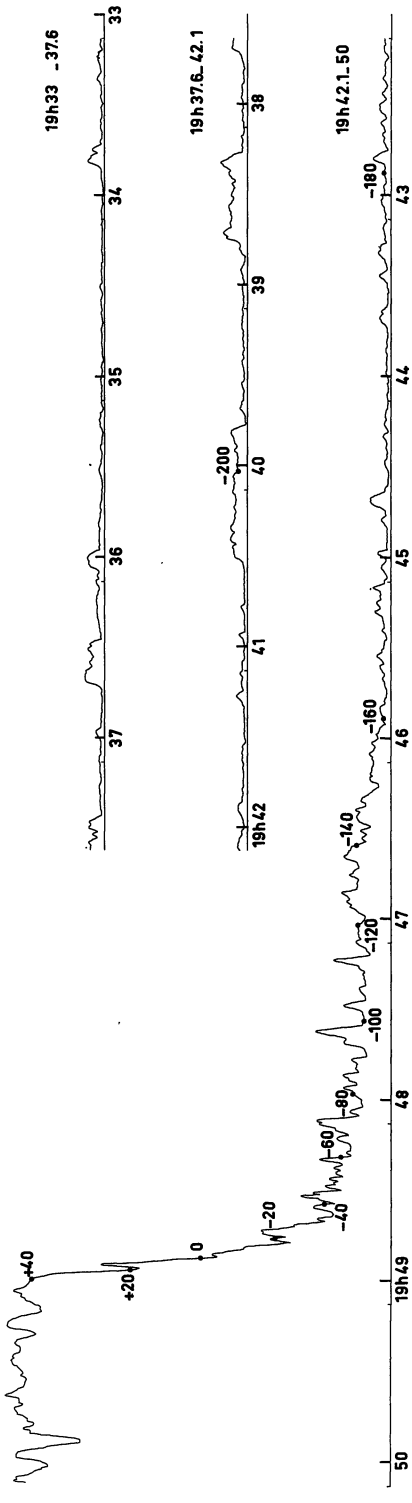

Fig. 2. The light curve, $\Phi(t)$, of β SCO A at Emersion, from 19 h 33 to 19 h 50 (U.T.). The time axis is reversed (time increases from right to left). The altitudes h corresponding to the points of closest approach are marked at 20 km intervals down to $h = -200$ km. Note the wide «plateaus», particularly between 19 h 36 and 19 h 40, and the rapid rise in flux after 19 h 46

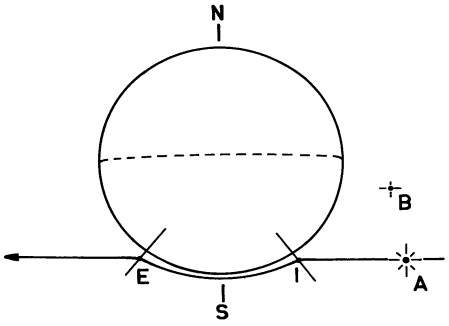

Fig. 3. A schematic representation of the refraction of the light from β SCO A by Jupiter's atmosphere. S is the south pole of Jupiter

errors, seeing and changes in the Earth's atmospheric transparency, this background level is not constant. We have then to effectively restrict this planetary background and to subtract what remains as carefully as possible.

To meet these requirements, we have used a three channel photometer: to increase the contrast between the star light and the planetary background, a narrow interference filter in the Ca II K-line and a circular aperture, as small as seeing allowed, were linked to the first channel. An annular mirror, surrounding this aperture, supplied the second channel with flux from Jupiter which may be related to the unwanted planetary background. The transparency of the Earth's atmosphere was continuously monitored in the third channel, in blue light.

Figures 1 and 2 show the occultation light curves at, respectively, immersion and emersion, after correction for the transparency of the Earth atmosphere and subtraction of the flux due to Jupiter. Inspection of these figures reveals numerous "spikes" in the first part of the curves and «plateaus» at the end. The light curve was recorded for more than 900 s at immersion and for more than 820 s at emersion. Visual guiding was continuously performed during this recording. When the star was too faint to allow visual guiding, offset guiding was performed, based on predictions for a Jovian atmospheric scale height of 25 km. The corresponding part of the light curve is neither presented nor analyzed in this paper.

Figure 3 gives the apparent location of the star during the occultation event.

II. The Method of Analysis

In this section we derive the relations that permit the atmospheric parameters – the refractive index and the altitude – to be deduced from the occultation parameters: the impact parameter and the bending angle. Then we show how these occultation parameters are deduced from the input data: the location of the star and the residual stellar flux as functions of time.

a) Basic Assumptions

The measured weakening of starlight during the occultation does not uniquely determine the spatial distribution of refractive index in the planetary atmosphere. Some a priori assumptions are required.

The basic assumption that we make is that the atmosphere is spherically symmetric and $\mu(r)$ is a function only of r. This assumption implies that there does not exist any horizontal gradient of the index of refraction or, equivalently, that vertical gradients of refractivity are much larger than horizontal gradients.

Additional assumptions are that the star may be considered to be a point source, that the influence of extinction due to absorption or scattering is negligible, and that the atmosphere is assumed to be a perfect gas in hydrostatic equilibrium.

b) Transformation of the Observational Data to a Refractive Index Profile

The basic geometry of the star occultation experiment is illustrated in Fig. 4. The refractive index μ is a function of r. A light ray may be characterized by two parameters:

– the radius of closest approach r_0

– the impact parameter $p(r_0)$ which is invariant along a ray, by Bouguer's rule. This invariant is:

$$p(r_0) = \mu(r) \cdot r \cdot \sin i \,. \tag{1}$$

In particular, the form of this invariant outside of the atmosphere is: $p(r_0) = r_e \cdot \sin i_e$, the distance from the planetary center to the asymptotic ray path. At the point of closest approach we have $p(r_0) = \mu(r_0) \cdot r_0$ which gives the relation between the refractive index and the two characteristic parameters of a light ray.

In what follows, we shall denote $p(r_0)$ by p_0.

As the index of refraction increases with depth in the atmosphere, light rays are bent toward the planetary center. The total bending angle of a ray is denoted by $\omega(p_0)$. As this angle is dependent upon p_0, differential bending occurs and produces a defocusing of the signal energy.

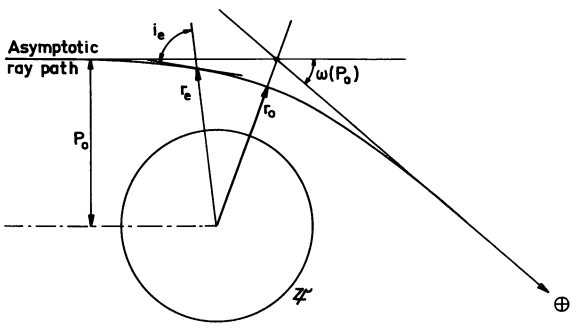

Fig. 4. Basic geometry of the star occultation

We have:

$$\omega(p_0) = \int_{r=r_0}^{\infty} \frac{2p(r)\cdot d\mu}{\mu(r)\cdot dr} \cdot \frac{dr}{\sqrt{[\mu(r)\cdot r]^2 - [\mu(r_0)\cdot r_0]^2}}. \quad (2)$$

Integral inversion of the Abelian Eq. (2) is performed to obtain the index of refraction at the altitude r_0. This procedure yields the following formula:

$$\mu(r_0) = \exp\left\{\frac{1}{\pi}\int_{\omega=0}^{\omega=\omega(p_0)} \mathrm{Log}\left[\frac{p(\omega)}{p_0} + \sqrt{\left(\frac{p(\omega)}{p_0}\right)^2 - 1}\right]\cdot d\omega\right\} \quad (3)$$

where

$$r_0 = p_0/\mu(r_0). \quad (4)$$

For a detailed discussion, the reader is referred to Phinney and Anderson (1968) or Fjeldbo *et al.* (1971).

$p(r_0)$ and $\omega(p_0)$ are in turn deduced from the imput data which are, in a star occultation experiment, the position of the star relative to the planetary limb and the residual stellar flux as functions of time.

As can be seen in Fig. 5, the location of the star relative to the planetary limb may be described by the Earth's motion relative to Jupiter, assuming the planet as stationary. As we assume that there does not exist any horizontal gradient of refractivity, the incident light ray and the refracted ray define a plane which is that of Fig. 5, where $z(t)$ is measured normally to the star direction.

Then, we have:

$$p(t) = R + z_{occ} - z(t) + D[\omega(t) - \omega(t_{occ})] \quad (5)$$

where the time of the half-power light level is taken as the origin of the time scale; R is the planetary radius at this level and D is the distance from Jupiter to the Earth.

The differential bending of light rays is related to the residual stellar flux by:

$$\frac{\Phi_0}{\Phi(t)} = -\frac{dz(t)}{dp(t)} \quad (6)$$

where Φ_0 is the stellar flux before the occultation and $\Phi(t)$ is the residual stellar flux as function of time.

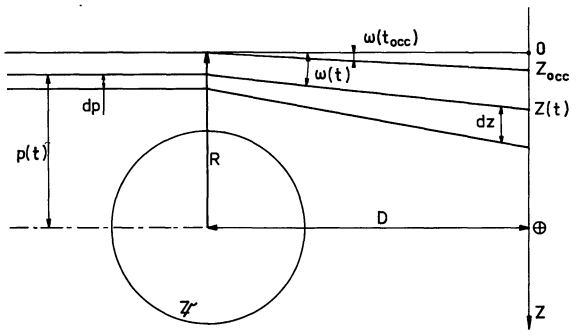

Fig. 5. Basic geometry of the star occultation. The subscript "occ" refers to the half-power level

Deriving Eq. (5), we obtain:

$$dp(t) = -dz(t) + D\cdot d\omega(t). \quad (7)$$

From (6) and (7) we deduce:

$$d\omega(t) = \frac{1}{D}\cdot\left[\frac{\Phi_0 - \Phi(t)}{\Phi_0}\right]\cdot dz(t). \quad (8)$$

The integration of which yields:

$$\omega(t) = \frac{1}{D}\cdot\int_{-\infty}^{\tau=t} \frac{\Phi_0 - \Phi(\tau)}{\Phi_0}\cdot dz(\tau). \quad (9)$$

In summary, the input data $\Phi(t)/\Phi_0$ and $z(t)$ are used to determine $p(t)$ and $\omega(t)$ from Eqs. (5) and (9). $p(t)$ and $\omega(t)$ are in turn used as imput data in the inversion relations (3) and (4), from which the vertical refractivity profile is obtained:

$$\nu(r_0) = \mu(r_0) - 1 \quad (10)$$

c) Temperature and Density Profiles

Vertical profiles of temperature and density can been obtained from the distribution of the index of refraction in the Jovian atmosphere.

The refractivity of the mixture H_2–He is given by:

$$\nu(h) = \sum_i K_i n_i(h) \quad (11)$$

with $i = H_2$ or He and where h, n_i, K_i denote the altitude, the number density and the molecular refractivity of each gas. We assume that other constituents are negligible. The half-power light level is taken as the origin of the altitude scale.

Two cases have been considered. The first one is a quite good representation of the Jovian atmosphere below the turbopause: the atmosphere is completely mixed at each level and is assumed to be an ideal gas in hydrostatic equilibrium. The second is a rough approximation only to the diffusive separation which takes place in the outer atmospheric layers. This approximation should be sufficient for our purpose: owing to the gravitational separation, each constituent, assumed to be an ideal gas, follows the hydrostatic law with its own scale height.

We have:

Case I

$$dp(h) = -n_t(h)\cdot\bar{m}\cdot g(h)\cdot dh \quad (12)$$

and

$$\frac{dp(h)}{p(h)} = \frac{dn_t(h)}{n_t(h)} + \frac{dT(h)}{T(h)} \quad (13)$$

with $n_t(h) = \sum_i n_i(h)$, $\bar{m} = \sum_i \frac{m_i\cdot n_i(h)}{n_t(h)}$, and where $p(h)$ is the pressure, $T(h)$ is the temperature, $\bar{m}$ is the mean molecular mass and $g(h)$ is the acceleration due to

gravity. From (12) and (13) one can deduce:

$$\frac{dn_t(h)}{n_t(h)} = -\frac{dT(h)}{T(h)} - \frac{\bar{m}\cdot g(h)\cdot dh}{k\cdot T(h)}. \quad (14)$$

Case II

$$dp_i(h) = -n_i(h)\cdot m_i\cdot g(h)\cdot dh \quad (15)$$

and

$$\frac{dp_i(h)}{p_i(h)} = \frac{dn_i(h)}{n_i(h)} + \frac{dT(h)}{T(h)} \quad (16)$$

with $i = H_2$ or He and where $p_i(h)$ is the partial pressure and m_i the molecular mass of each constituent.
From (15) and (16) one can deduce:

$$\frac{dn_i(h)}{n_i(h)} = -\frac{dT(h)}{T(h)} - \frac{m_i\cdot g(h)\cdot dh}{k\cdot T(h)}. \quad (17)$$

On eliminating the pressure from Eqs. (12, 13) or (15, 16), Eq. (11) may be written:

$$\frac{dv(h)}{v(h)} = -\frac{dT(h)}{T(h)} - \frac{F(h)\cdot g(h)\cdot dh}{v(h)\cdot k\cdot T(h)} \quad (18)$$

with

$$F(h) = \sum_i \bar{m}\cdot K_i\cdot n_i(h) = \bar{m}\cdot v(h) \quad \text{in Case I}$$

or

$$F(h) = \sum_i m_i\cdot K_i\cdot n_i(h) \quad \text{in Case II.}$$

The vertical profiles of temperature and number density are obtained by integrating (18) and (14) or (17) using the trapezoidal rule.
Two points should be noted:
– as mentioned above, the basic assumption concerning the atmospheric structure is that horizontal gradients of refractivity are much smaller than vertical gradients.
– in order to integrate (18) and (14) or (17) boundary conditions are needed: the temperature $T(h_0)$ and the mixing ratio $q(h_0)$ at the arbitrary chosen altitude h_0. The level h_s at which gravitational separation occurs must be fixed.

III. The Refractivity Profile and Typical Profiles of Temperature and Number Density

In the following section are present typical temperature and number density profiles derived from the refractivity profile which we have obtained.

a) The Jovian Refractivity Profile

The vertical refractivity profiles $\log v(h)$ obtained at the immersion and the emersion of β Sco A, are shown in Fig. 6. The trapezoidal rule is used for the numerical integration of (3) and (9). As noted above, the level of the half occultation is taken as the origin of the altitude scale.

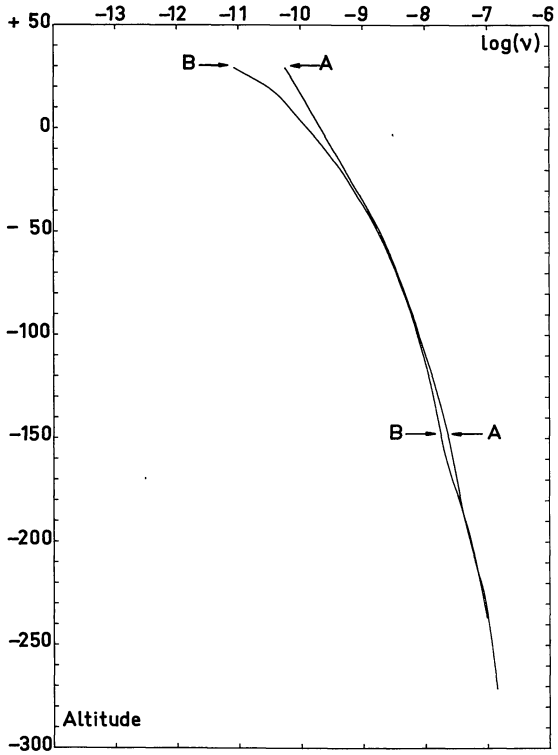

Fig. 6. Refractivity profiles $\log(v(h))$ obtained at Immersion (A) and Emersion (B). Note the divergence between the two profiles above the altitude $h = 0$

We wish to comment on several points:
– The measurements cover heights over more than 200 km and over a refractivity range from about 10^{-12} to 10^{-7}.
– As shown by the strong departure of the refractivity profile from a linear law, the atmosphere cannot be isothermal. The overall convex shape of the profile is quite similar to that observed in the atmosphere of Venus during the Mariner V occultation experiments (Fjeldbo *et al.*, 1971). This shape reveals a strongly negative temperature gradient, $\frac{dT}{dh}$.
– It should be noted that the profiles $v(h)$ obtained at the immersion and at the emersion are in good agreement. Nevertheless, the divergence increases above the altitude $h = 0$ because of the difference in shape between the two light curves during the first seconds of the immersion and the last seconds of the emersion (Berezné *et al.*, 1974; see Fig. 1, Fig. 2).
– Also note that, the deeper one observes in the atmosphere, the smaller are the irregular inflexions of the refractivity profile due to the "spikes" on the light curves.
– The departure from a linear law of $\log v(h)$ which we have deduced is larger than that obtained by Hubbard *et al.* (1972). For the highest levels that they probed, Hubbard *et al.* deduced a value of the refractivity

close to 10^{-10} or 10^{-11} and a related altitude of $+120$ km. From our light curves and for the same decrease in stellar flux, we deduce a refractivity close to 10^{-11} or 10^{-12}, the related altitude lying between $+40$ and $+50$ km. This strong disagreement is due to the importance of noise in the upper part of the light curves more than significant differences in their shape.

In our experiment the residual stellar flux, $\Phi(t)/\Phi_0$, which is used as input data in relations (6) and (9), is provided by the observed light curves. The time constant, one half the time constant of the photometer, is $\delta t = 0.5$ s. As the Earth's atmospheric fluctuations yield a noticeable noise level, the departure of $\Phi(t)/\Phi_0$ from unity is not significant before $t = -10$s. This time has been chosen as origin of the integral inversion ($t = -10$s). The advantage of such a procedure is to avoid any smoothing of the upper part of the light curves; but it implies the unrealistic assumption that zero pressure is reached at a finite altitude, close to $+100$ km, in the Jovian atmosphere. (Clearly, $\Phi(t)/\Phi_0 = 1$ is an asymptotic value in a quasi-exponential atmosphere.) Consequently the computed refractivity in the upper atmospheric layers is underestimated and decreases too rapidly with altitude. The problem here is to estimate the uncertainty $\Delta\nu$ we introduce in assuming the noisy light curve to be the actual light curve: the computed values of $\nu(h)$ deduced from (3) and (10) have to be increased by a constant, $\Delta\nu^*$, independent of altitude, as can be easily shown, if the upper layers are assumed to be isothermal.

$$\Delta\nu^* = \left[\frac{\Phi_0}{\Phi^*} - 1\right] \cdot \frac{H_0}{D} \cdot \left[\frac{H_0}{2\pi R}\right]^{1/2} \tag{19}$$

where $\frac{\Phi^*}{\Phi_0}$ is the actual value of the residual stellar flux at $t = -10$ s and H_0 is the scale height of the outer atmosphere. We may choose, as the most probable value of the temperature in the assumed isothermal outer atmosphere, $T_0 = 150$°K which is the temperature we obtained for the quasi-isothermal region lying between 0 and -50 km (see Section V).

An extreme value may be $T = 300$ °K which slightly exceeds the theoretical value given by Shimizu (1971). With $g = 26.5\ \mathrm{m \cdot s^{-2}}$ and $\bar{m} = 2.3$, the scale heights are 20 and 40 km respectively. Taken into account the noise level, and estimating Φ^* by eye on the light curve, we obtain:

Φ^*/Φ_0	Most probable value	Upper limit
Immersion	0.980	0.950
Emersion	0.985	0.965

The related values of $\Delta\nu^*$ are

$\Delta\nu^*$	Most probable value	Upper limit
Immersion	$4 \cdot 10^{-12}$	$3 \cdot 10^{-11}$
Emersion	$3 \cdot 10^{-12}$	$2 \cdot 10^{-11}$

Figure 7 shows the corrected refractivity profiles. The intriguing curvature of the function $\log \nu(h)$ in the

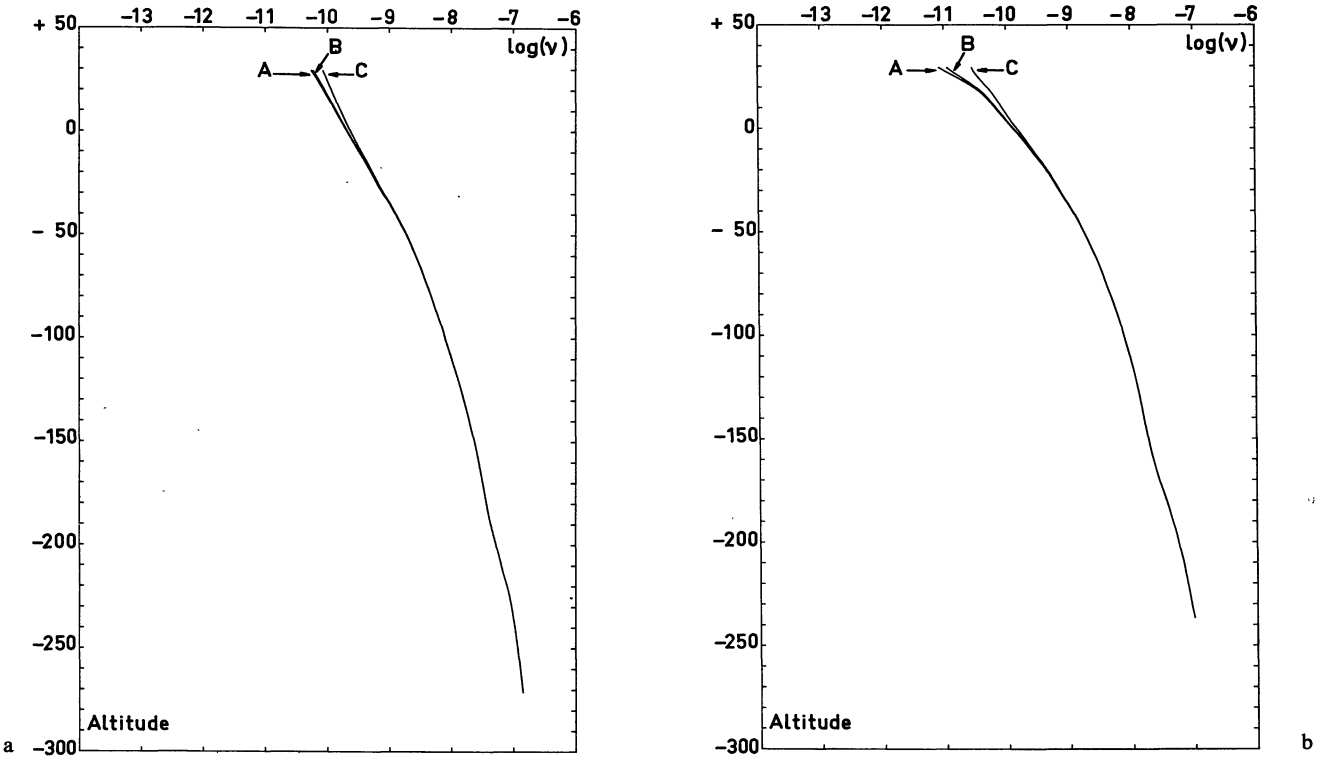

Fig. 7 a and b. Corrected refractivity profiles. a Immersion. A: $\Delta\nu^* = 0$; B: $\Delta\nu^* = 4 \cdot 10^{-12}$; C: $\Delta\nu^* = 3 \cdot 10^{-11}$. b Emersion; A: $\Delta\nu^* = 0$; B: $\Delta\nu^* = 3 \cdot 10^{-12}$; C: $\Delta\nu^* = 2 \cdot 10^{-11}$

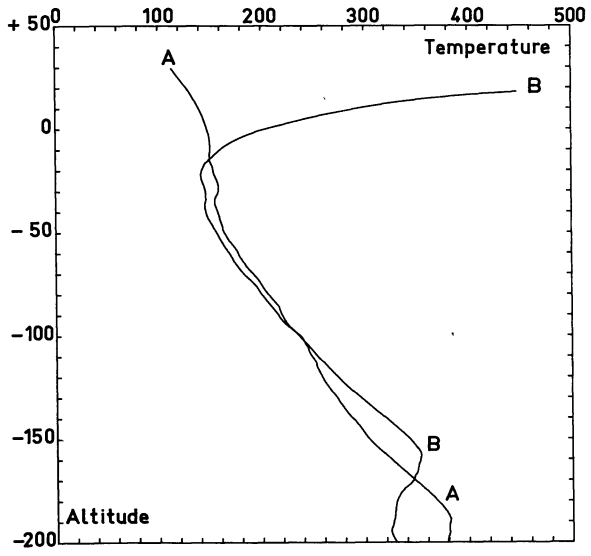

Fig. 8. Typical temperature profiles, $T(h)$, obtained at Immersion (A) and Emersion (B). $q=0.9$; $h_0=-14$ km; $T_0=150$ °K. Note the temperature maxima at $h=-190$ km (A) and -160 km (B)

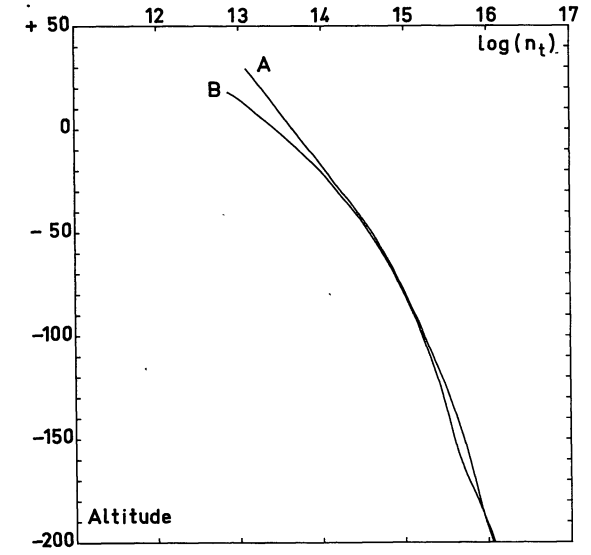

Fig. 9. Typical density profiles $\log(n_t(h))$, obtained at Immersion (A) and Emersion (B). $q=0.9$; $h_0=-14$ km; $T_0=150$ °K. Since ν and n_t are proportional if the atmosphere is well mixed, i.e. the mixing ratio is altitude independent, Fig. 9 and Fig. 6 are similar

outer layers disappears and a linear extrapolation of the refractivity profile obtained between $h=-50$ km and $h=+20$ km may be a realistic representation of $\log \nu(h)$ above $+20$ km.

In conclusion, the noise due to atmospheric seeing prevents the refractivity in the outer atmosphere being obtained. The correction $\Delta\nu^*$, discussed above, is no more than an estimate of the uncertainty as a function of altitude. It adds no information in itself.

In what follows, we have used the profiles $\log \nu(h)$, directly deduced from the observed light curves without any correction $\Delta\nu^*$; but all the results concerning the vertical profiles of the temperature and the density are restricted to the altitudes less than 30 km, where the uncertainty in the refractivity reaches 100%.

b) Typical Temperature and Number Density Profiles

Figures (8) and (9) show typical results of the numerical integration described in Section 2. The vertical profiles of temperature presented here were obtained assuming the atmosphere to be homogeneous with $q=0.9$. The boundary conditions are:

$h_0=-14$ km and $T(h_0)=150$ °K.

The influence of these boundary conditions will be discussed in Section IV. Figure 8 shows the temperature profiles of the atmosphere during the immersion and the emersion of β Sco A. The level of half occultation is taken as the origin of the altitude scale. The altitude decreases in the direction of the center of Jupiter. Figure 9 gives the corresponding vertical distribution of the number density.

The temperature is nearly constant from the occultation level to $h=-50$ km. Then it increases with depth in the atmosphere. The lapse-rate is approximately -1.5 °K/km. A maximum of temperature is reached at nearly 200 km under the occultation level. All the profiles of temperature that we shall present are quite similar. In comparing the immersion and emersion profiles, we note that the temperature lapse-rate at the sunset side (immersion) appears to be slightly higher than it is at the sunrise side (emersion). Inspection of Fig. 8 reveals a fine structure in the temperature profiles. While the absolute value of the temperature may be in error by 50 °K, as will be shown below, these small temperature variations are nevertheless significant. It should be noted that the numerous small "spikes" which are prominent features of the light occultation curves do not yield visible temperature changes in the plotted profiles (see Section IV).

IV. Limits of the Probe of the Atmospheric Layers and Error Analysis

The present section is concerned first with the determination of the limits of the observations of Jupiter's atmosphere.

a) The Upper Limit

The integration of Eq. (14) or (17) yields

$$T(h)=T(h_0)\cdot\frac{n_t(h_0)}{n_t(h)}+\frac{1}{k\cdot n_t(h)}\cdot\int_{h'=h}^{h'=h_0}\bar{m}(h')\cdot g(h')\cdot n_t(h')\cdot dh'. \tag{20}$$

The boundary temperature $T(h_0)$ can be arbitrarily chosen and influences the computed temperature profile. As $n_t(h)$ is roughly proportional to the refractivity $\nu(h)$

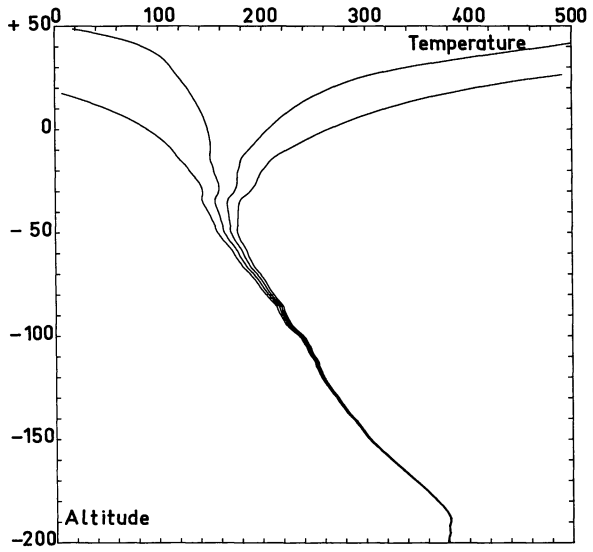

Fig. 10. The influence of the integration parameters T_0 and h_0 upon the deduced temperature profile at Immersion. $q=0.9$; $h_0=-14$ km; $T_0=120$, 150, 180, 210 °K. The profile is independent of T_0 for $h<-100$ km.

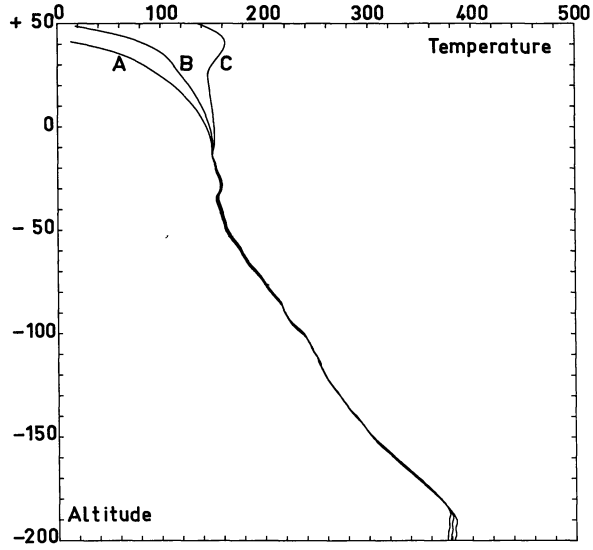

Fig. 11. The influence of a 1% error in the flux level of β SCO A upon the temperature profile at Immersion. A Φ_0 increased by 1%; B Reference curve; C Φ_0 decreased by 1%. $q=0.9$; $h_0=-14$ km; $T_0=150$ °K. The profile $T(h)$ is significantly affected only high in the atmosphere ($h>0$ km)

even if the atmosphere is not well-mixed one can see that the influence of $T(h_0)$ becomes rapidly negligible as deeper atmospheric levels are probed. In contrast, its influence increases strongly with increasing altitudes as shown in Fig. 10.

In addition to the influence of $T(h_0)$, the uncertainties in the photometric data introduce severe limitations on the validity of the computed temperatures in the outer atmospheric layers. As discussed previously, the thermal and density profiles are determined from the refractive index, which in turn is determined from the ray bending angle $\omega(t)$ and the impact parameter $p(t)$. As shown by Eqs. (9) and (5) these quantities depend on the integral of the residual stellar flux $\Phi(t)$. Thus, while local errors in the light curve (or spikes) will result in negligible changes in temperature and density, uncertainties in the determination of the stellar flux before the occultation, Φ_0, on the other hand, strongly affect the thermal and density profiles. Figure 11 shows how they are affected when error limits on Φ_0 are $\pm 1\%$, as seems to be the case in our experiment (Berezné *et al.*, 1974). One can see that above the altitude $h=+30$ km, the error on $T(h)$ may exceed 100 °K.

Lastly, we have to remember that the uncertainty in $v(h)$ reaches 100% at the altitude $h=+30$ km (see Section III.a).

In view of the above discussion [influence of T_0, uncertainties in Φ_0 and $v(h)$] the upper limit of h for which useful results have been obtained is $h=+30$ km.

b) The Lower Limit

Let us now analyse the influence of an error in the determination of the zero-light level. As seen above (Fig. 1) the stellar flux decreases rapidly as deeper atmospheric layers are probed. In these layers, an error in the zero level introduces an important relative error in the residual stellar flux and thus in $T(h)$ as deeper and deeper levels are considered. Figure 12 shows the influence of an error of $\pm 1\%$ in the zero light level. It can be seen that the vertical profiles are strongly affected for $h \leqq -200$ km.

Another fact could invalidate the temperature determination below $h=-200$ km. The location of the point of the ray closest approach is shown on Fig. 13. As can be seen, the altitude of the point of closest approach decreases very slowly, except during the first minute, while the related horizontal displacements are of thousands of kilometers. One must, therefore, ask if the horizontal changes in refractive index remain much smaller than the vertical variation.

First a point should be made: most of the refractive bending occurs in the vicinity of the point of closest approach. It can be shown than 95% of the refractive bending is due to a ray path of 8000 km in the Jovian atmosphere as seen in Fig. 13 (Combes *et al.*, 1972). To perform the integral inversion, we must assume spherical symmetry or, in others words, that along an atmospheric path of 8000 km horizontal changes in refractivity remain much smaller than the vertical changes. Now, a horizontal displacement of 8000 km from the half-occultation point is related, as can be seen in Fig. 13, to a decrease in altitude of nearly 200 km. Thus, we must assume that horizontal changes in refractivity are much smaller than vertical changes above $h=-200$ km. It would be hazardous to extend this assumption to deeper atmospheric layers.

A second point is that inspection of the light curve $\Phi(t)$ corresponding to altitudes less than $h=-200$ km

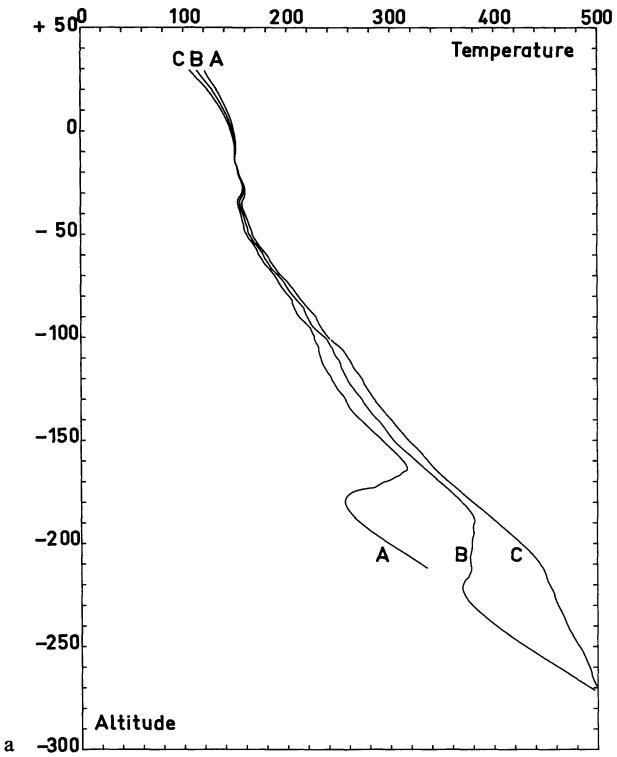

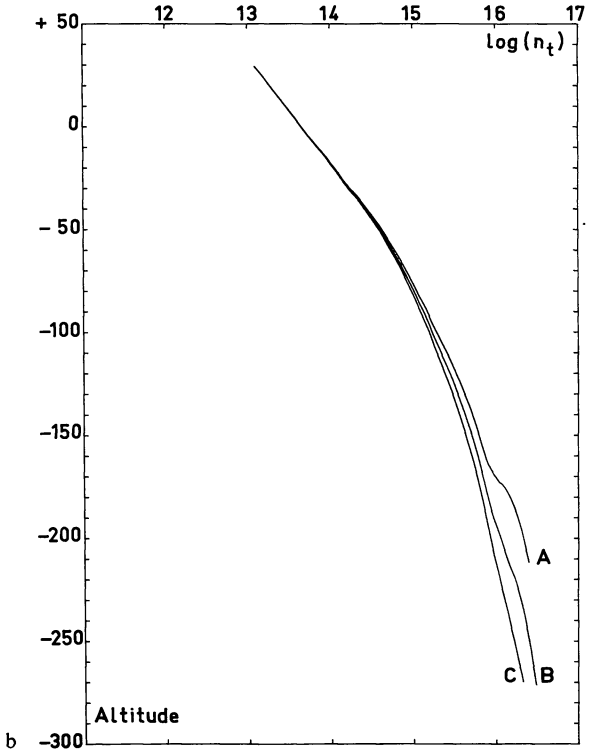

Figs. 12a and b. The influence of a error in the Jovian background light upon the temperature profile and the density profile at Immersion. A Background light level increased by $\Phi_0/100$; B Reference curve; C Background light level decreased by $\Phi_0/100$. $q = 0.9$; $h_0 = -14$ km; $T_0 = 150$ °K. The profile $T(h)$ is appreciably affected deep in the atmosphere ($h < -100$ km). Note the displacement of the temperature maximum

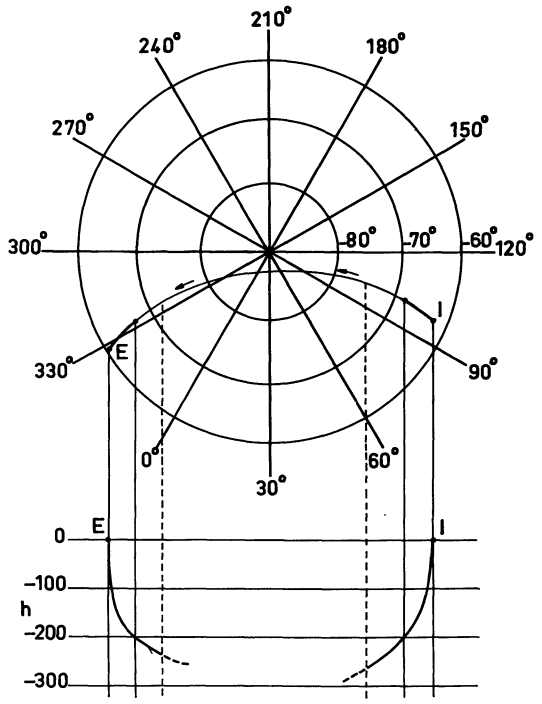

Fig. 13. Trajectory of the point of closest approach of the ray path. *Top*: Map of the south polar region of Jupiter from $-90°$ to $-60°$ in zenographic latitude and for all longitudes λ_{II}. I is the Immersion and E the Emersion point. The heavy curves correspond to altitudes $-200 < h < 0$ km. *Bottom*: Corresponding variation in h. $dh/dt = -3.9$ km · s^{-1} at $h = 0$, -0.1 km · s^{-1} at $h = -200$ km

reveals characteristic features (see Fig. 1 and 2). From place to place, the residual stellar flux increases significantly for 10s or more. Such features are like rather broad "plateaus" of emission. Assuming the atmosphere to be spherically symmetric at the corresponding levels yields incredibly high temperatures. As the features observed during immersion are not time-symmetric with those occurring during emersion, and as the horizontal displacement of the point of closest approach greatly exceeds its vertical displacement, we should be careful when assuming that horizontal changes in refractivity remain much smaller than vertical changes below $h = -200$ km. A more realistic interpretation of such features may be that local refractivity irregularities are due to local density or temperature fluctuations.

In conclusion, in view of the uncertainties described above, the adopted limits of the analysis of the atmospheric layers are $h = +30$ km and $h = -200$ km. Therefore, the analysis of a thermosphere or of the atmosphere below the maximum of temperature is very doubtful, if spherical symmetry is assumed. The data we have obtained at the minimum of the residual stellar flux, in the polar region of Jupiter, and which are related to atmospheric layers below $h = -200$ km, will be analysed separately in a forthcoming paper.

c) Error Analysis

Systematic errors are believed to be significantly reduced by taking account of a number of effects.

1. The star velocity, normal to the planetary limb, is computed as function of time. At immersion, for example, it decreases from 7.7 km/s when $h=0$ km to 6.2 km/s when h reaches -200 km.

2. The Jovian ellipticity is taken into account in the following way: spherical symmetry is assumed at any given time t, but the parameter R used in Eq. (5) is the instantaneous radius of curvature of the ellipsoid in the ray path plane. The equatorial radius and oblateness are taken from Lecacheux *et al.*, (1972) for an angular separation of β Sco A – C equal to 13.60″, and R is computed as a function of time. For example, at immersion, R increases from 75640 km to 76040 km when h goes from zero to -200 km. The consequence of this correction is that the derived value of the refractivity increases as deeper atmospheric layers are probed, but the correction remains smaller than 1% even at $h=-200$ km.

3. The variation of the acceleration due to gravity with both the altitude and the latitude has also been taken into account. Using data given by Michaux (1967), one can compute that g increases from 26.60 m · s^{-2} at $h=0$ to 26.97 m · s^{-2} at $h=-200$ km. At this level, the temperature derived by this procedure differs by 5 °K from the temperature obtained using a constant value of g.

4. A more significant factor is the influence of the flux from β Sco B, which lies 0.4″ from β Sco A, on the derivation of $v(h)$ and $T(h)$. According to Hubbard and Van Flandern (1972) the flux of β Sco B in blue light should not exceed 1% of the flux of β Sco A and may be neglected. However, as we have shown in Section IV,

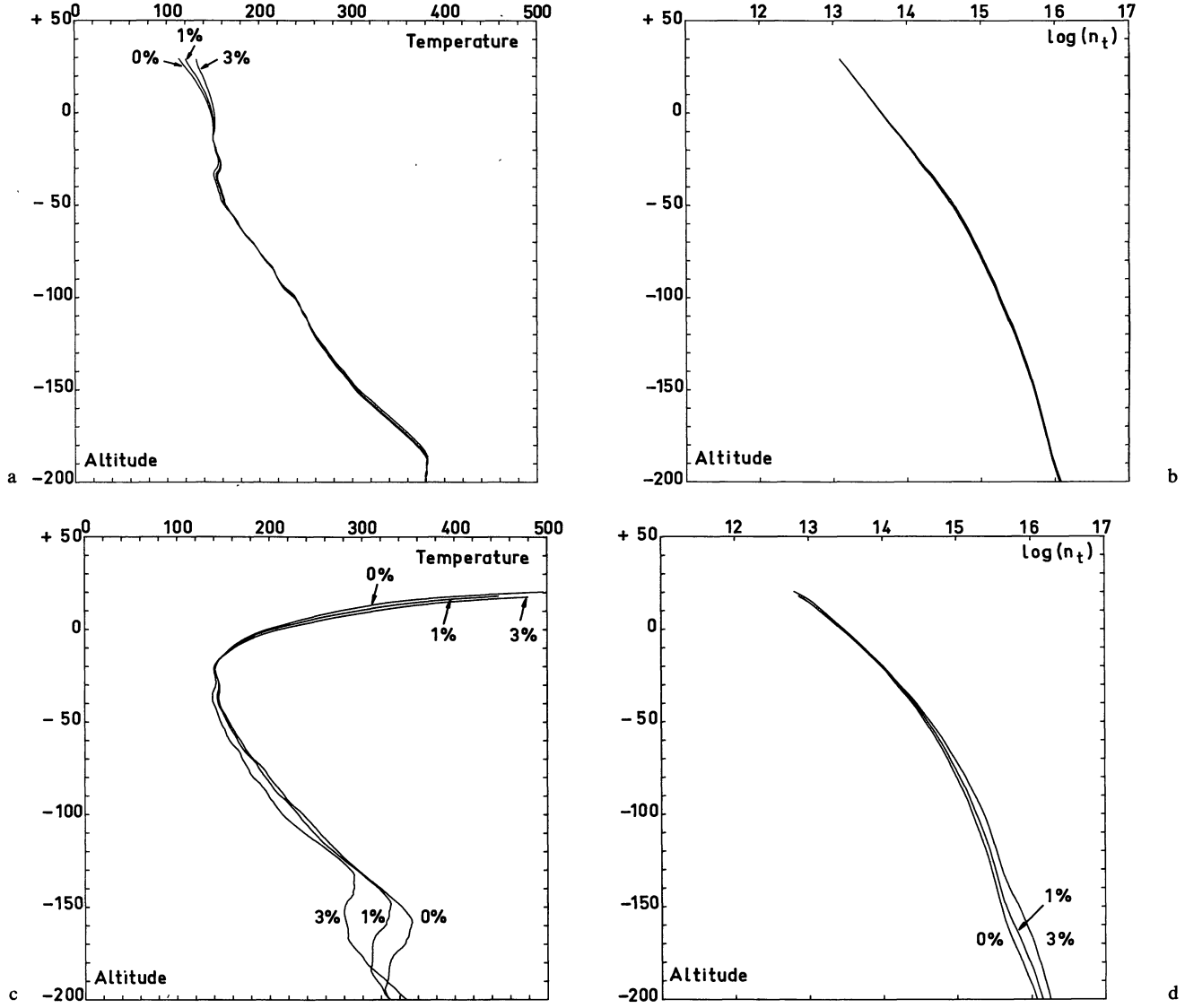

Figs. 14 a – d. Influence of an error in the relative intensities of stars β SCO A and β SCO B : $B/A=0\%, 1\%, 3\%$. $q=0.9$; $h_0=-14$ km; $T_0=150$°K. a and b Immersion. a Temperature profiles; b Density profiles. c and d Emersion. c Temperature profiles; d Density profiles

an underestimation of the zero-level of the stellar flux by about 1% leads to 100 °K lower temperatures in the deeper atmospheric layers. Moreover, according to Kuiper (1935) or Van den Bos (1951, 1960), β Sco B is brighter than is ordinarily accepted: $V=5$ to 7 rather then $V=9$ or 10.

To establish the size of the resulting systematic error, we have computed the refractivity and temperature profiles obtained from the observed light curve, assuming that it results from the addition of the light curves of the two stars. The light curve of B Sco B is obtained, to sufficient accuracy, by reducing the observed light curve in the ratio of the fluxes of the two stars before the occultation. In our computer program, the times of the half-occultation events of β Sco B are determined on assuming that the location of β Sco B relative to β Sco A is $\varrho=0.4''$ and $\theta=140°$ (Hubbard and Van Flandern, 1972). Subtracting the computed light curve of β Sco B from the observed light curve, we derived the corrected light curve relating to β Sco A. As the timings of the half occultation events of the two stars do not differ by more than 15 s, the change in the refractivity and temperature profiles at immersion are probably unimportant. In contrast, owing to the fact that the difference in the timings at the emersion exceeds 2 min and that the emersion of β Sco B occurs when the flux of β Sco A is still very low, noticeable changes in the resulting profiles are to be expected. Figure 14 shows the consequence of neglecting β Sco B, assuming a blue magnitude of 6.4 and 7.6: the atmosphere may be 30 °K colder at the level $h=-150$ km. As can be seen, the divergence between the immersion and emersion temperature profiles is increased by taking into account β Sco B (the discrepancy remains for any value of the magnitude of β Sco B).

V. Conclusions Concerning the Jovian Upper Atmosphere

The adopted limits in the analysis of the upper Jovian atmosphere having been specified and the influence of the main sources of inaccuracy discussed, we are now able to present some conclusions. The following questions will be considered:

1. May the H_2/He mixing ratio be estimated from our experiment?
2. What is the range of temperature and the lapse rate in the probed layer?
3. Does there exist a temperature maximum, and, if so, what is its value and its location?
4. Do our measurements provide any new data on the thermosphere? Are they at variance with previous analyses?
5. Are there significant differences between the immersion and emersion regions?

As seen above, the relation (9) giving the temperature as function of the altitude depends on the boundary constant, $T(h_0)$. Although its influence on the computed profile becomes rapidly negligible with depth, we have, nevertheless, to choose realistic values for T_0 and h_0. The altitude $h_0=-14$ km has been arbitrarily chosen. The related number density $n_t(h_0)$ is close to 10^{14} cm^{-3} and the relative uncertainty in the refractivity $\Delta\nu/\nu$ is only a few percent (see Section III). A temperature of $T_0=150$ °K is probably a realistic value because it is close to the temperature of the quasi-isothermal region lying between 0 and -50 km (see Section V, 2).

a) The H_2/He Mixing Ratio

Figure 15 gives a set of temperature profiles for different mixing ratios: $0.7\leqq q\leqq 1.0$. The two most important effects of an increased abundance of helium are:

– First, the temperature profile above $h=0$ km is strongly modified. A slight increase in the mixing ratio

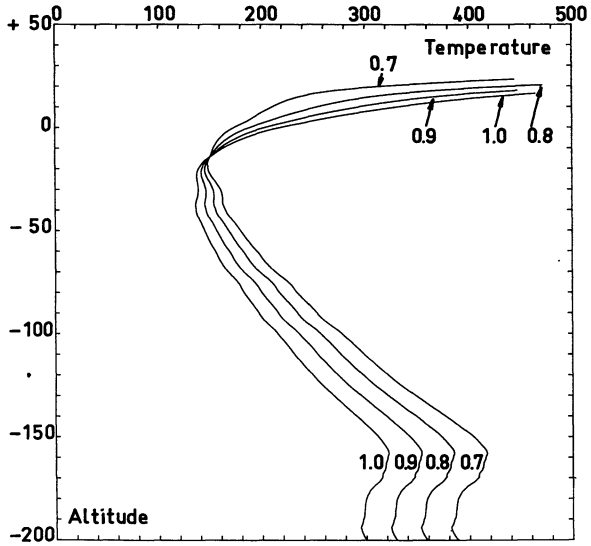

a

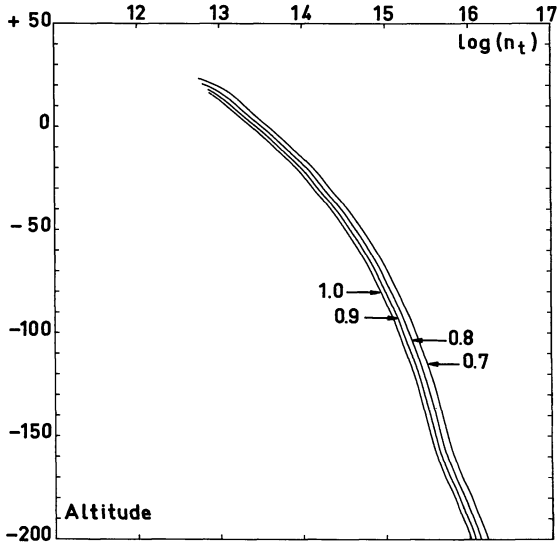

b

Figs. 15a and b. Influence of the mixing ratio, $q=H_2/H_2+He$, at Emersion. $q=1.00$ (A), 0.90 (B), 0.80 (C), 0.70 (D); $h_0=-14$ km; $T_0=150$ °K. Temperature profiles; Density profiles

produces a large decrease in the lapse-rate. The outer atmospheric layers are significantly colder than they would be in the case of a pure hydrogen atmosphere.

– Secondly, the mean lapse-rate between the levels -50 km and -150 km becomes greater. It increases by a factor of 1.3 when the abundance of helium is increased from 0% to 30%. Larger abundances of helium would result in unacceptable values of the temperature.

We may conclude, only, that helium is not a major component of the Jovian atmosphere. Thus we cannot confirm nor refute the conclusion of Owen and Mason (1968), who deduced from their observations of hydrogen in the (3.0) and (4.0) bands that q exceeds 0.8.

b) The Temperature Range and the Lapse-rate above $h = -50$ km

In this region, the temperature profile is largely determined by the choice of boundary condition. We have assumed that values of T_0 resulting in temperatures less than 80 °K at $h = +30$ km may be excluded. Similarly, an upper limit to T_0 may be obtained on assuming that $T(h)$ must be less than 400 °K [this value exceeds by 100 °K the higher temperature computed by Shimizu (1971)].

Figure 16 shows the temperature profiles for a set of values of T_0, assuming $q = 0.9$. As we have seen above, the inaccuracy in the refractivity becomes important at

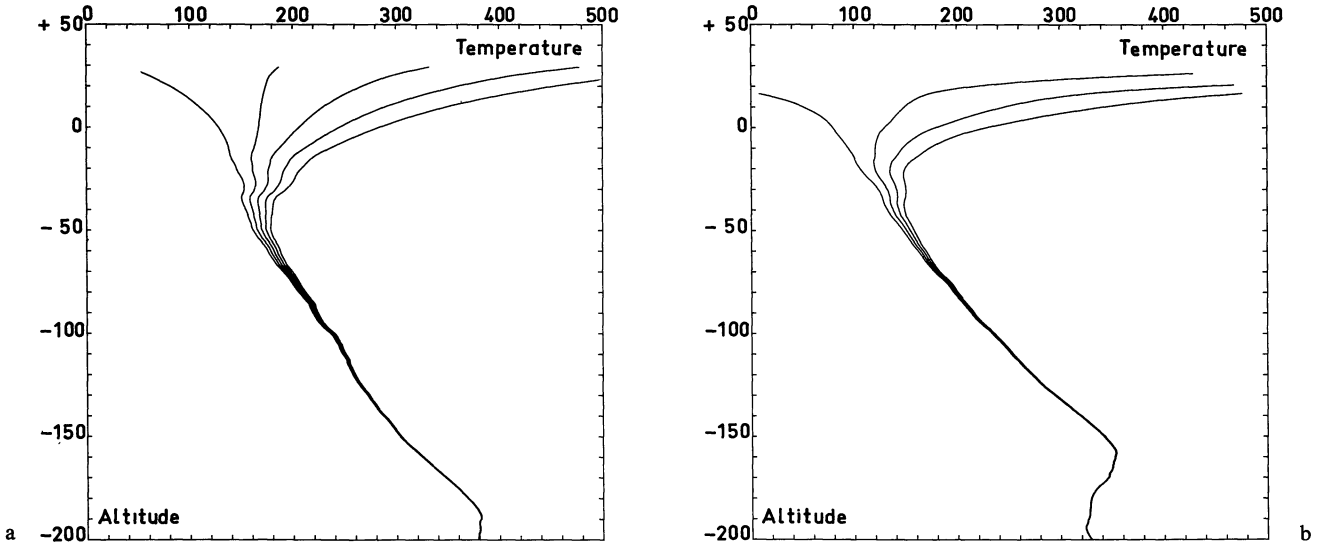

Figs. 16a and b. Temperature profiles assuming $q = 0.9$, $h_0 = -14$ km. a Immersion. $T_0 = 140$, 160, 180, 200, 220 °K. b Emersion. $T_0 = 100$, 120, 140, 160 °K

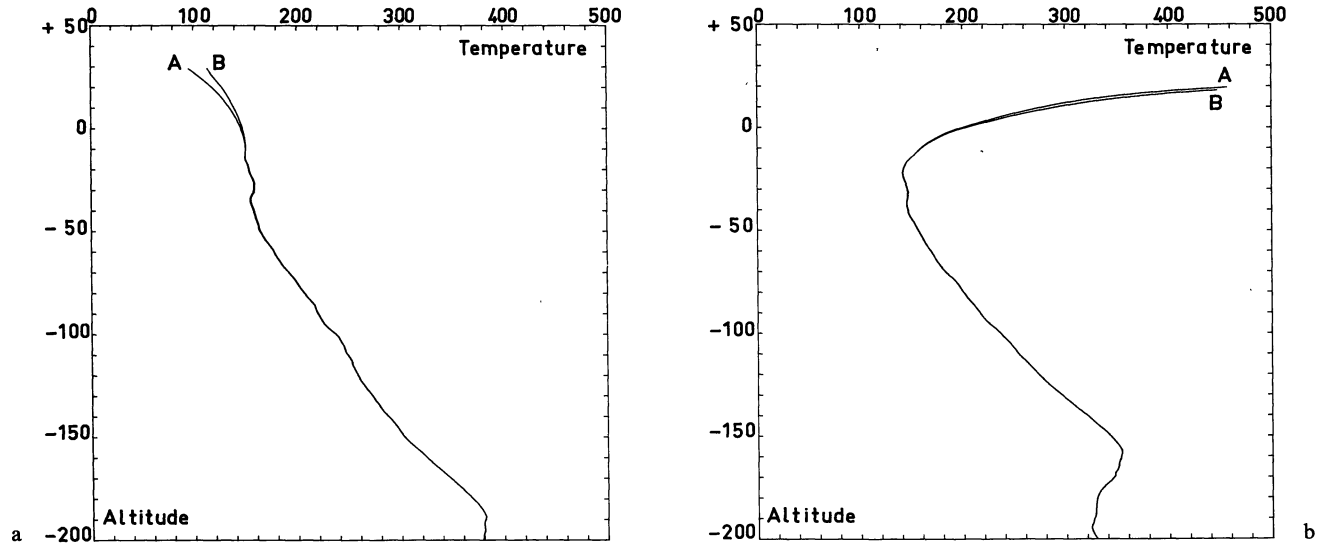

Figs. 17a and b. Influence of the correction Δv^* upon the temperature profiles. $q = 0.9$; $h_0 = -14$ km; $T_0 = 150$ °K. a Immersion. A $\Delta v^* = 4.10^{-12}$; B Reference curve ($\Delta v = 0$). b Emersion. A $\Delta v^* = 3.10^{-12}$; B Reference curve ($\Delta v^* = 0$)

these altitudes. Figure 17 gives the temperature profiles when the correction Δv^* is added (see Section IV).
From inspection of these curves we conclude that:
$150 \leqq T_0 \leqq 220$ °K at immersion, and
$100 \leqq T_0 \leqq 150$ °K at emersion.
If we accept that the mixing-ratio lies between 1.0 and 0.7, these temperature ranges must be enlarged as following:
$130 \leqq T_0 \leqq 240$ °K at immersion, and
$100 \leqq T_0 \leqq 170$ °K at emersion.
The influence of the altitude of the homopause has also to be taken into account. Assuming a hydrogen dominated atmosphere (140 °K) and taking CH_4 as the main radiating molecule, McGovern and Burk (1971) have computed the number density at the level at which the diffusive separation of H_2 and He begins to occur. Their results lie between $n = 2 \cdot 10^{12}\,\mathrm{cm}^{-3}$ and $n = 2 \cdot 10^{14}\,\mathrm{cm}^{-3}$, depending on the assumed value of the eddy diffusion coefficient. These densities correspond to the layer $(-40, +60$ km) in our altitude scale. Figure 18 shows the temperature and density profiles at immersion for a set of altitudes of the homopause and for $q = 0.9$. The profile is quasi-isothermal, for a well-mixed atmosphere, between -50 and $+50$ km. If diffusive separation takes place, a strong negative gradient $\frac{dT}{dh}$ occurs, at one scale height above the level h_s. This effect becomes more pronounced in the outer layers as the abundance of helium decreases with respect to hydrogen.

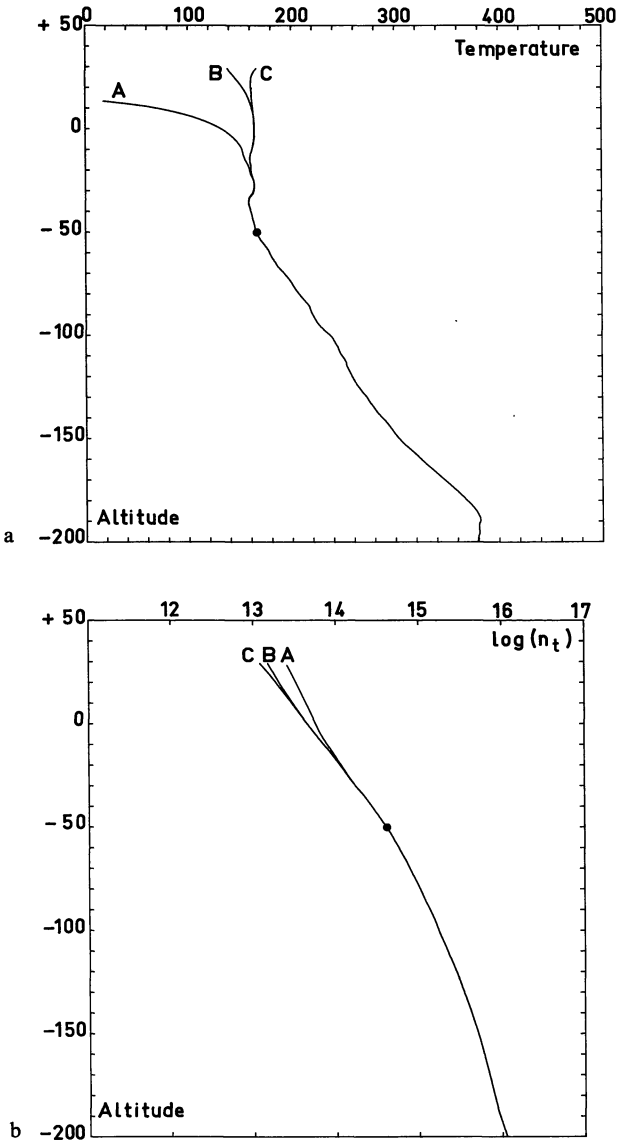

Figs. 18 a and b. Temperature profiles and Density profiles for a set of altitudes of the homopause, h_S, at Immersion. $q = 0.9$; $h_0 = -50$ km; $T_0 = 165$ °K. A $h_s = -40$ km; B $h_s = -10$ km; C $h_s = +20$ km

We may conclude that the homopause level may be located as deep as $h = -40$ km, in agreement with theoretical computations by McGovern and Burk. In this case, the extremely large temperature lapse-rate which occurs above $h = -20$ km might be greatly reduced or even suppressed.
In conclusion, whatever the boundary temperature T_0 may be, it is possible to choose either q or h_s to obtain, between -50 and $+30$ km, a quasi-isothermal profile (150 to 170 °K) or a slightly positive lapse-rate ($+0.25$ °K/km) similar to those computed by McGovern and Burk or Shimizu. Because of this uncertainty and because the analysis of the atmosphere above $h = 30$ km is quite impossible (see IV, a), it follows that the occultation of β Sco cannot provide any information about the Jovian thermosphere. Therefore, the increase of temperature noted by Hubbard *et al.* (1972) on their J 3 and NT 3 profiles is not significant, and the observation of β Sco occultation is not in contradiction with the theoretical analysis of McGovern and Burk or Shimizu.

c) The Temperature and the Lapse-rate between -50 km *and* -150 km

Figure 8 shows that the temperature lapse-rate, between -50 and -150 km ($2 \cdot 10^{-9} \leqq v \leqq 2 \cdot 10^{-10}$), is nearly constant and close to $\frac{dT}{dz} = -1.6\,^{\circ}\mathrm{K} \cdot \mathrm{km}^{-1}$. This result depends only on q. A fact to be noted here is that the immersion and emersion profiles yield similar results for both the lapse-rate and the extent of the linear part of $T(h)$.
Hubbard *et al.* (1972) obtained a negative gradient of the scale height for $v > 10^{-8}$. At the altitude $h = -100$ km, the related temperature lapse-rate is $\frac{dT}{dz} = -0.8^{\circ}\,\mathrm{K} \cdot \mathrm{km}^{-1}$. Because of the appreciable uncertainty in the residual stellar flux due to the Jovian background, one might ascribe the divergence, by a factor 2, to a difference in the estimates of the zero level of star light (see Section IV). However, as shown in Fig. 12, this uncertainty has no appreciable effect upon the temperature lapse-rate. We consider the slight

difference in shape of the light curves obtained in Johannesburg and in Pretoria to be the source of the discrepancy in the lapse-rates. At immersion, the flux measured between +15 and +50 s by Hubbard *et al.* decreases more rapidly than in our measurements and β Sco becomes approximately 20% fainter. This difference may be due to actual differences in the Jovian atmosphere in spite of the fact that the regions observed from Johannesburg and from Pretoria are distant by no more than some tens of kilometers.

d) The Maximum of Temperature

As the temperature exceeds 200 °K with a negative lapse-rate between −50 and −150 km and as the temperature at the cloud level must be close to 150 °K, a maximum of temperature may be postulated.

The vertical profiles which we have obtained actually show a maximum of $T(h)$ at $h = -190$ km and −160 km at immersion and emersion, respectively. The question is whether this maximum is significant and what is the accuracy of the related values of T_M, h_M and n_M.

The conclusions of our analysis are:

– a maximum of temperature exists in the probed layers whatever the choice of the different parameters;

– it is located so deep that the adopted value of T_0 has no influence on the value of T_M;

– the altitude h_M of the maximum depends strongly on the accuracy of the determination of the zero light level of the star. An error of ±1% in this level results in a change Δh_M of the altitude h_M: $\Delta h_M = +30$ km and −100 km, respectively. The related error in the temperature T_M is close to 100 °K.

Of special interest is the fact that, from the light curves published by Hubbard *et al.* (1972) or by Veverka *et al.* (1972) and from temperature profiles presented by Wasserman (1973), it appears that these authors have estimated the zero level of star light as being reached more rapidly than do we. In other words, the planetary background is assumed to be more important in their data reduction than in ours. Consequently, the temperature of the maximum must be less and it must be located higher in the atmosphere. However, we believe our zero level and related uncertainty range (±1%) to be correct, not only because they result from our analysis of the photometric data (Berezné *et al.*, 1973) but also because of the appearance of the characteristic features described in Section IV. We cannot exclude the possiblity that a systematic error may result in both an underestimate of the planetary background and in the appearance of these characteristic features, but none has been disclosed until now.

Using our estimate of the upper value of the planetary background, we are able to give an upper limit to the altitude h_M. We obtain $h_M \leqq -160$ km and $h_M \leqq -130$ km at immersion and emersion, respectively. As seen above, the value of T_M depends strongly on the zero light level, but it depends also on the mixing ratio. As the term $T_0 \frac{n_t(h_0)}{n_t(h)}$ in relation (20) may be neglected at such a depth, it follows that T_M is proportional to $\bar{m}$. A lower limit to T_M, assuming $q = 1$, is $T_M \geqq 280$ °K and $T_M \geqq 260$ °K at immersion and emersion, respectively. In a similar way, we obtain $n_M \geqq 7 \cdot 10^{15}$ cm^{-3}, $P_M \geqq 0.3$ mb at immersion and $n_M \geqq 3 \cdot 10^{15}$ cm^{-3}, $P_M \geqq 0.1$ mb at emersion, as lower limits to the number density and the pressure at the temperature maximum.

e) Comparison between Immersion and Emersion Results

Immersion and emersion temperature profiles differ significantly.

A differential effect due to latitude could have some importance. The location of the half-immersion and half-emersion points are −62.7° and −60.8° respectively. (Zenographic latitudes, see Fig. 13). The related shift from North to South is close to 2600 km. Also note the occurrence of a differential effect due to change in the insolation: owing to the small value of the phase angle (2.0°) on the 13th of May 1971, the point of closest approach of a light ray (Fig. 13) closely follows the terminator throughout the occultation event. The distance from the point of closest approach to the terminator never exceeds 1200 km. Due to the great heigt of the occultation level above the clouds, the atmospheric layers responsible for the occultation were outside of the planetary umbra. However, immersion occurs 0.4 h before sunset and emersion 0.4 h after sunrise, and insolation change may have played a significant part in the temperature difference.

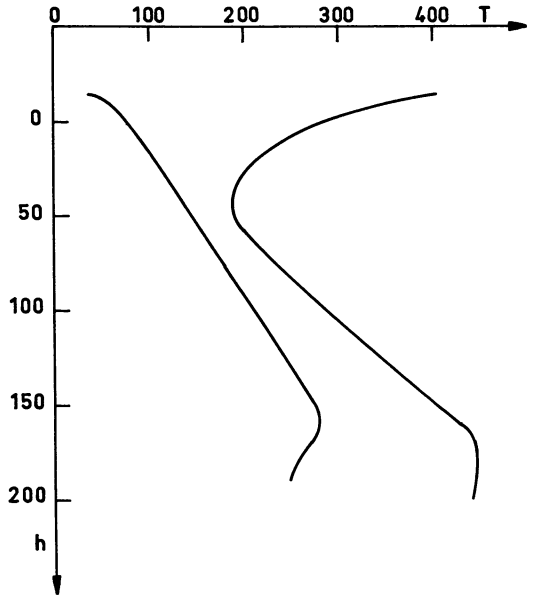

Fig. 19. The uncertainty in T as function of altitude

Summary and Conclusion

The most important results of our experiment are summarized in Fig. 19:
– the temperature lapse-rate is close to $-1.5\ °K \cdot km^{-1}$ between the levels -50 km and -150 km;
– the temperature at $h = -100$ km is 220 ± 30 °K, if we accept that the abundance of helium is less than 20%;
– below this layer a maximum of temperature is reached, but we cannot accurately determine its location, the pressure at this point may be close to 1 mb and the temperature to 300 or 400 °K;
– above the altitude $h = -50$ km, the thermal lapse-rate decreases to zero and a quasi-isothermal layer may exist ($T = 150 \pm 50$ °K);
– above $h = 20$ km the temperature and the lapse-rate cannot be defined. It is impossible to obtain any information on the thermosphere.

Appendix I

μ	refractive index
r	distance to the planetary center
r_0	radius of closest approach
$p(r_0)$ or p_0	impact parameter
i	angle of incidence of a light ray with respect to a normal to the planet
r_e	any distance to the planetary center outside of the atmosphere
i_e	angle of incidence at r_e
$\omega(p_0)$	total bending angle of the light ray having p_0 as impact parameter
$z(t)$	Earth's motion normal to the star direction
R	planetary radius at the half occultation level
D	distance from Jupiter to the Earth
$\omega(t)$	total bending angle at any given time t
$\omega(t_{occ})$	total bending angle at the half occultation time
Φ_0	stellar flux before occultation
$\Phi(t)$	stellar flux at any given time t
$\nu(r_0)$	refractivity at distance r_0
h	altitude – the half occultation level is taken as origin of the altitude scale
$\nu(h)$	refractivity at the altitude h
K_i	molecular refractivity of each constituent
$n_i(h)$	density number of each constituent
$p(h)$	pressure at altitude h
$n_t(h)$	total density number
$\bar{m}$	mean molecular mass
$g(h)$	acceleration due to gravity at altitude h
m_i	molecular mass of each constituent
$T(h)$	temperature at altitude h
$\mathscr{R}$	gaz constant
k	Boltzmann's constant
$p_i(h)$	partial pressure of each constituent
h_0	altitude at which the boundary conditions are chosen
$T(h_0)$	boundary temperature
q	mixing ratio ($H_2/H_2 + He$)
h_s	altitude of the homopause
$\Delta\nu^*$	correction factor of the refractivity
Φ^*/Φ_0	actual value of the residual stellar flux at $t = -10$s
H_0	scale height of the outer atmosphere
T_M	maximum of temperature
h_M	altitude of the maximum of temperature
n_M	density number at h_M
p_M	pressure at h_M
$\frac{dT}{dh}$	temperature lapse-rate

Acknowledgements. Our warm thanks are due to Dr. Thackeray, Director of Radcliffe Observatory, and his staff for very helpful assistance. We are grateful to J. L. Heudier for liaison with the Radcliffe Observatory.

References

Berezné, J., Combes, M., Laporte, R., Lecacheux, J., Vapillon, L. 1974, to be published
Combes, M., Lecacheux, J., Vapillon, L. 1971, *Astron. & Astrophys.* **15**, 235
Fjeldbo, G., Kliore, A. J., Eshleman, V. R. 1971, *Astron. J.* **76**, 2, 123
Hubbard, W. B., Nather, R. E., Evans, D. S., Tull, R. G., Wells, D. C., Van Citters, G. W., Warner, B., Vanden Bout, P. 1972a, *Astron. J.* **77**, 41
Hubbard, W. B., Van Flandern, T. C. 1972b, *Astron J.* **77**, 65
Kuiper, G. P. 1935, *Publ. Astron. Soc. Pacific* **47**, 25
Lecacheux, J., Combes, M., Vapillon, L. 1973, *Astron. & Astrophys.* **22**, 289
Mac Govern, W. E., Burk, S. D. 1971, *J. Atmos. Sci.* **29**, 179
Michaux, C. M. 1967, Handbook of the Physical Properties of the Planet Jupiter, NASA, Washington
Owen, T., Mason, H. P. 1968, *Astrophys. J.* **154**, 317
Phinney, R. A., Anderson, D. L. 1968, *J. Geophys. Res.* **73**, 1819
Shimizu, M. 1971, *Icarus* **14**, 273
Van den Bos, W. H. 1951, Circ. Union Obs., No. 111, 13, 1960, Circ. Union Obs., No. 119, 321
Veverka, J., Elliot, J., Sagan, C., Wasserman, L., Liller, W. 1972, *Nature* **240**, 344
Wasserman, L. 1973, 3d Annual Meeting of the Division for Planetary Sciences of the A.A.S. (Tucson)

L. Vapillon
M. Combes
J. Lecacheux
Groupe «Planètes»
Observatoire de Meudon
F-92190 Meudon, France